

# A Route to Ultra-Fast Amplitude-Only Spatial Light Modulation using Phase-Change Materials

Joe Shields, Carlota Ruiz De Galarreta, Harry Penketh, Yat-Yin Au, Jacopo Bertolotti, and C. David Wright\*

A phase-change material based, thin-film, amplitude-only spatial light modulator is presented. The modulator operates in reflection and modulates the amplitude of light incident on its surface with no effect on optical phase when the phase-change material is switched between its amorphous and crystalline states. This is achieved using a thin-film device with an embedded, switchable, GeTe phase-change layer. Test modulation patterns are written to the device using laser scans, and the amplitude and phase response measured, using optical spectroscopy and off-axis digital holography. Experimental results reveal reflected intensity to be modulated by up to 38%, with an averaged phase difference of less than  $\approx \pi/50$ . Since phase-change materials such as GeTe can be switched on sub-microsecond timescales, this approach maps out a route for ultra-fast amplitude spatial light modulators with widespread applications in fields such as wavefront shaping, communications, sensing, and imaging.

devices,<sup>[6]</sup> and digital micromirror devices (DMDs).<sup>[7,8]</sup> LCoS spatial light modulators (SLMs) primarily control the optical phase of light interacting with them,<sup>[9,10]</sup> and operate at relatively low modulation speeds, typically in the low 100s of Hz.<sup>[8]</sup> Issues with LCoS SLMs include crosstalk between neighbouring pixels and phase flicker.<sup>[11]</sup> Digital micromirror devices offer modulation speeds orders of magnitude faster than those of LCoS systems, typically up to tens of kHz.<sup>[12]</sup> However, micromirrors essentially modulate only the intensity of light in a binary on-off manner, though non-binary intensity modulation can be achieved using pulse-width-modulation techniques.<sup>[12]</sup> In spite of many advances in the capabilities of such SLM devices in recent years, full wavefront control

with conventional SLM approaches can only be achieved via holography.<sup>[13]</sup> Holographic approaches are however rather inefficient, as a large part of the light is diffracted away, and only a fraction goes in the desired wavefront. The currently missing tool to enable efficient full optical wavefront control is a device capable of performing amplitude-only modulation, and one which could be easily coupled to a phase-only modulator.

Stand-alone optical amplitude modulation is also important for many other practical applications across a range of areas including optical-based sensing, imaging, communications and computing. Motivated by this fact, over recent years there has been much attention given to pursuing novel strategies for the design and implementation of active amplitude modulation based on reconfigurable nanophotonic devices. These include metasurfaces and thin film layer stacks incorporating materials whose refractive indices can be actively and dynamically switched or tuned via appropriate thermal, electrical, or optical stimuli.<sup>[14,15]</sup> Amongst the variety of available materials, chalcogenide phase-change materials (PCMs) are arguably one of the most attractive options.<sup>[14]</sup> Chalcogenide PCMs are alloys consisting of at least one chalcogen element (usually Te), and can be rapidly (nanosecond timescale<sup>[16]</sup>) and repeatedly (potentially as many as  $10^{15}$  cycles<sup>[17]</sup>) switched between their amorphous and crystalline states. Such states exhibit markedly different optical (refractive index) and electrical (conductivity) properties, as well as being non-volatile. Crystallization of PCMs generally requires heating to moderately elevated temperatures somewhere above the “static” crystallization temperature (approximately 180 °C for bulk GeTe<sup>[18]</sup>) but below melting temperature; this is

## 1. Introduction

The ability to control the amplitude and phase of optical wavefronts has many important scientific and technological applications, such as beam steering, image processing, optical mode conversion, compensation for scattering or aberrations, and optical computation, to name but a few (see, e.g., Refs. [1–4] and also Pinho et al.<sup>[5]</sup>, Chapter 7)). The most commonly adopted approaches to such wavefront control include liquid crystal spatial light modulators, in particular liquid crystal on silicon (LCoS)

J. Shields, H. Penketh, Y.-Y. Au, J. Bertolotti, C. D. Wright  
Centre for Metamaterial Research and Innovation  
University of Exeter  
Exeter EX4 4QF, UK  
E-mail: david.wright@exeter.ac.uk  
C. R. De Galarreta  
Laser Processing Group  
Instituto de Optica  
IO-CSIC, Serrano 121, Madrid 28006, Spain

The ORCID identification number(s) for the author(s) of this article can be found under <https://doi.org/10.1002/adom.202300765>

© 2023 The Authors. Advanced Optical Materials published by Wiley-VCH GmbH. This is an open access article under the terms of the Creative Commons Attribution License, which permits use, distribution and reproduction in any medium, provided the original work is properly cited.

DOI: 10.1002/adom.202300765

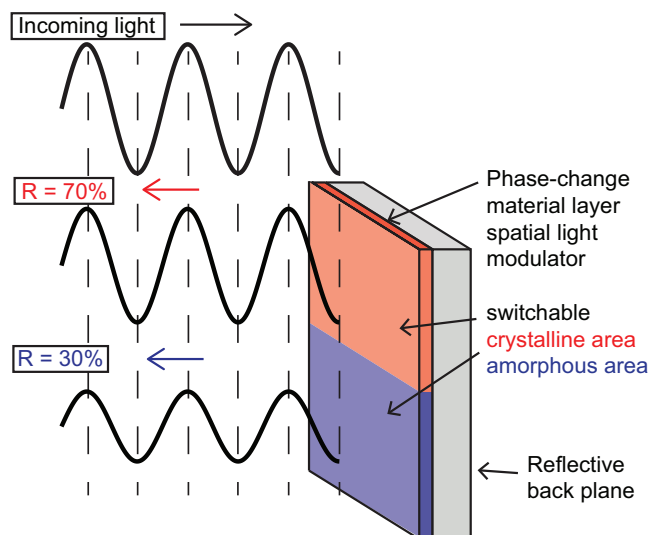


**Figure 1.** Schematic of device operation showing an example of a region (or pixel) having the PCM layer switched into its crystalline state, and another into the amorphous state. Reflected light is strongly modulated in amplitude, but has near-zero phase difference upon reflection between amorphous and crystalline regions.

typically achieved using relatively low power and/or relatively long duration heat stimuli. The amorphization process requires the material to be heated above its melting temperature (725 °C for bulk GeTe<sup>[19]</sup>) and then for it to be rapidly cooled to quench it into its less energetically favourable amorphous state. This is achieved via the use of relatively short excitations,<sup>[14,20,21]</sup> ideally carried out over small PCM volumes surrounded by good thermally conductive materials to increase the cooling rates.<sup>[16,22,23]</sup> In addition, fractionally crystallized states can also be reached by carefully controlled heat stimuli, so yielding multi-level tunability of the complex refractive index or electrical conductivity.<sup>[22,24]</sup>

To date, the combination of PCMs with micro- and nanophotonic devices has been extensively and successfully applied to active and multi-level amplitude control of optical beams in different spectral regimes, including the visible, near- and mid-infrared.<sup>[22,23,25,26]</sup> Such existing approaches are typically based on optically resonant structures such as metasurfaces and Fabry-Perot cavities<sup>[22,27,28]</sup> and although providing excellent amplitude control, such control is invariably accompanied by significant changes in the optical phase, preventing their direct application to amplitude-only modulation.

In this work, therefore, we demonstrate the concept of a “true” amplitude-only modulator using a phase-change material based approach. Contrary to other PCM-based approaches reported in the literature, our devices have been designed to operate off-resonance, resulting in amplitude modulation being accompanied by virtually no changes to the optical phase. As generically depicted in **Figure 1**, the design is based on a simple (thus cost-effective and readily-integrated) reflector with a PCM thin-film layer (here GeTe), providing a tunable optical environment. Our devices have been successfully designed and fabricated, and their performance in terms of optical amplitude and phase modulation has been tested via optical spectroscopy and an off-axis digital holography interferometer. Experiments carried out on laser-

written (modulated) devices revealed absolute modulation depths of 38% upon GeTe crystallization (an extinction ratio of 3.5, where extinction ratio is defined as  $ER = -10\log_{10}(R_{am}/R_{cry})$ ), accompanied by near-zero changes in the optical phase (below  $\approx\pi/50$ ). We believe our findings point the way toward a new class of fast (MHz switching rates), practicable, cost-effective, and non-volatile amplitude-only spatial light modulators, in turn potentially enabling the realization of a simple approach to full optical wavefront control and manipulation.

## 2. Results and Discussion

### 2.1. Amplitude-Only Constant-Phase Modulator Design Platform

Our phase-change material based amplitude-only modulators have been designed to operate in reflection and at a central wavelength of 632.8 nm. Other wavelengths are readily accessible by suitable device re-design and/or change of PCM composition. A wide range of PCM compositions exhibiting different wavelength dependant optical properties are currently available.<sup>[14]</sup> Schematics of the devices are shown in **Figure 2a**. The devices consist of a 100 nm thick titanium back reflector with a thin GeTe layer above, covered with a 5 nm thick upper ITO layer to prevent oxidation. From the available PCM alloys, GeTe was chosen as the active material due to its superior optical extinction coefficient ( $k$ ) contrast between amorphous and crystalline states. This in turn will lead to high reflectance contrast at the wavelength of interest.<sup>[29]</sup> The complex refractive index used in this work was obtained via ellipsometry of as-deposited and hot plate annealed GeTe, and is shown in **Figure 2b**. Titanium was chosen as a reflector due to its high melting point (1668 °C), which is well above the melting point of GeTe (725 °C). This ensures robustness against the temperatures required to amorphize the GeTe layer. Titanium also possesses a high thermal conductivity, which in turn facilitates the high cooling rates required for successful amorphization of the GeTe layer. Finally, as previously stated, the ITO capping layer is primarily used as a transparent/conductive layer to protect the GeTe layer from oxidation which, in the case of GeTe, starts immediately when exposed to air<sup>[30]</sup> and has been proven to affect the optical and switching properties of the material.<sup>[31,32]</sup> In analogy to current SLM technology, and due to its inherent simplicity, our design platform is therefore ultimately compatible with implementation of a pixelated and electrically switchable device. Such electrical switching might be achieved by using the bottom metal plane and a top patterned ITO layer as electrodes for in-situ electrical switching,<sup>[33]</sup> or by patterning the metal layer to provide embedded micro-heaters,<sup>[34]</sup> with both approaches opening up the route to sub-microsecond operation.

### 2.2. Device Optimization and Analysis

Device optimization and analysis were carried out by introducing the generic geometry shown **Figure 2a** into the finite-element analysis package COMSOL Multiphysics (COMSOL, Inc., Stockholm, Sweden). Analyses were performed in 2D, employing the radio-frequency (RF) module in the frequency domain. Lateral boundaries were set as Floquet periodic conditions to mimic an

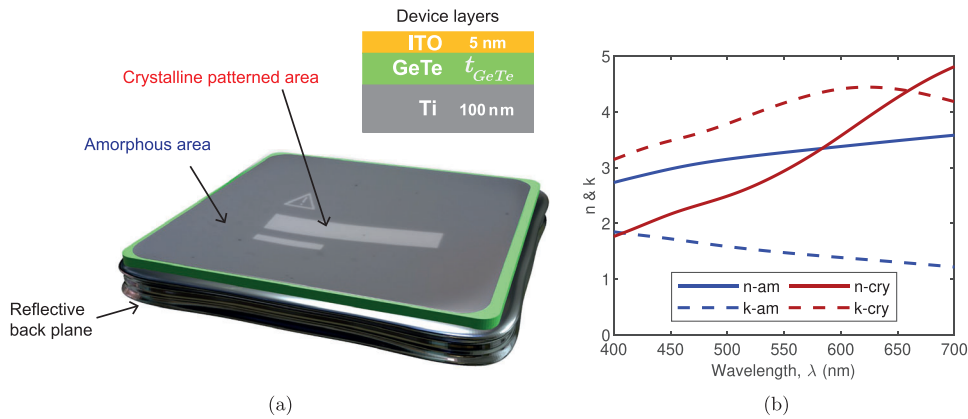


**Figure 2.** a) Schematic shows a 3D render of the device with a pattern written as a crystalline area of the PCM. This area has a significantly larger reflectance than the surrounding amorphous areas of the device. Generic device shown as a 2D cross section including layer materials and thicknesses: bottom reflecting Ti layer (100 nm), GeTe PCM layer thickness ( $t_{GeTe}$ ) and ITO capping layer (5 nm). Note that the GeTe layer thickness was optimized in simulation (see main text) to maximize amplitude modulation while simultaneously minimising phase modulation, the optimum thickness being 29 nm. b) Complex refractive index of GeTe obtained via ellipsometry measurements. Measurements were made of as-deposited GeTe (in its amorphous state) and crystalline GeTe (after annealing on a hot plate at 200°C for 10 min).

infinite surface, and electromagnetic excitation was carried out via a plane wave at normal incidence. Top (air) and bottom (Ti) domains were truncated by perfectly matched layers to avoid computational reflections from internal domains. Since the optical properties of a particular PCM composition can vary significantly depending on the deposition conditions,<sup>[35]</sup> the complex refractive index of our amorphous and crystalline GeTe films (shown in Figure 2b) was measured via ellipsometry over the range from 400 to 1600 nm. Other material property values were taken from the literature: Ti<sup>[36]</sup> and ITO.<sup>[37]</sup> Optimization of the layer stack to yield maximum amplitude modulation in tandem with minimum phase modulation was performed with a single variable, the thickness of the GeTe layer ( $t_{GeTe}$ ). The thickness of the Ti and ITO layers were held constant at values of 100 and 5 nm, respectively. The absolute modulation depth ( $\Delta R$ ) and optical phase delay ( $\Phi$ ) between amorphous, partially amorphous and crystalline states was monitored while varying the GeTe thickness. Intermediate GeTe states (i.e., between fully amorphous and fully crystalline states) were calculated using the Bruggeman-type effective medium model to approximate the dielectric constant ( $\epsilon$ ) of the mixed phase as follows:<sup>[38]</sup>

$$\epsilon(f, \epsilon_{am}, \epsilon_{cr}) = \frac{1}{4} \left[ 2\epsilon_p - \epsilon'_p + \sqrt{(2\epsilon_p - \epsilon'_p)^2 + 8\epsilon_{am}\epsilon_{cr}} \right] \quad (1)$$

with

$$\epsilon_p = (1-f)\epsilon_{am} + f\epsilon_{cr}, \quad (2)$$

$$\epsilon'_p = f\epsilon_{am} + (1-f)\epsilon_{cr} \quad (3)$$

where  $f$  is the fraction of crystallization and  $\epsilon_{am}$  and  $\epsilon_{cr}$  are the dielectric constants for GeTe in the amorphous and crystalline states, respectively.

The  $\Delta R$  and  $\Phi$  are defined as follows

$$\Delta R = |R_{cr} - R_{am}| \quad (4)$$

$$\Phi = \phi_{cr} - \phi_{am} \quad (5)$$

with  $R_{cr}$  and  $R_{am}$  being the reflectance in the crystalline and amorphous phases and  $\phi_{cr}$  and  $\phi_{am}$  being the relative phase differences in the crystalline and amorphous states.

Optimum GeTe thickness to maximize modulation depth upon crystallization while keeping the optical phase variation at a minimum (whilst limiting the GeTe layer thickness due to the challenge associated with the re-amorphization of larger PCM volumes) was found to be  $t_{GeTe} = 29$  nm. **Figure 3a** shows simulated performance of the designed devices as the fraction of crystallization increases. It can be seen that there is a high simulated modulation depth in reflection ( $\Delta R = 0.39$ ) and a very small optical phase difference (maximum of  $\Phi = \pi/150$  rad, as shown in inset of **Figure 3a**). The high modulation depth with virtually no phase difference between amorphous and crystalline states can be qualitatively explained in terms of the optical penetration depths of amorphous and crystalline GeTe at the wavelength of interest (632.8 nm). In the amorphous phase, the GeTe material has an optical penetration depth of 38 nm (linear absorption coefficient of  $0.026 \text{ nm}^{-1}$ ), which is close to the thickness of the GeTe layer (29 nm). In the crystalline phase, the penetration depth is even smaller, at 11 nm, due to the much larger extinction coefficient in the crystal phase. In combination with the bottom titanium layer, light entering the GeTe layer is thus attenuated in a single internal reflection roundtrip, and cannot re-radiate to free space. This prevents the formation of Fabry–Pérot cavity modes, whose optical phase is sensitive to changes in both the optical properties and thickness of the cavity. In other words, the GeTe layer can be considered as an optical bulk (thus off-resonance), and its reflectance in both amorphous and crystalline states is mainly dominated by Fresnel contributions at the GeTe/air interface (the ITO layer being optically thin (5 nm)), with negligible changes in reflected optical phase.

Finally, since SLM-based devices do not always operate at normal incidence (i.e., a specific tilt angle may be introduced, typically around  $0^\circ$  and  $30^\circ$  depending on the experimental

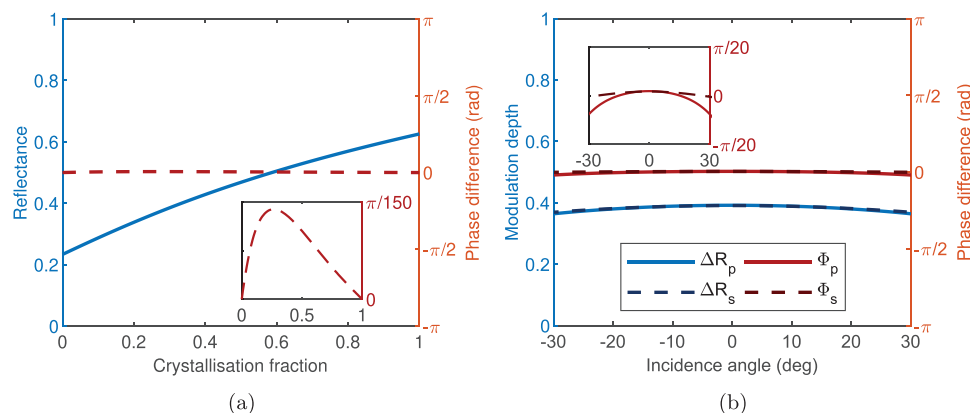


**Figure 3.** a) Simulation results showing the reflectance and phase difference upon reflection of optimized devices as the fraction of crystallization increases from 0 to 1. Modulation depths of 0.39 achieved with simulated near zero phase difference of reflected light between fully amorphous and crystalline devices. Inset shows magnified phase difference, a peak of  $<\pi/150$  radians of phase difference is seen at 26% fractional crystallization. b) Angle of incidence simulation results from  $-30^\circ$  to  $+30^\circ$ . Results show the change in reflectance  $\Delta R$  and change in phase  $\Phi$  for both p- and s-polarized light.

setup/specific application), robustness, in terms of varying the angle of incidence, was also investigated. This was done by carrying out simulations with light incident between  $0^\circ$  and  $30^\circ$  in both s- and p-polarizations. The results of these simulations can be seen in Figure 3b. The results show the devices have good robustness against varying the angle of incidence, with the phase difference upon switching increasing a small amount as the angle of incidence increases. At the extreme angle of  $30^\circ$  the maximum phase difference is found to be:  $\phi_p \approx \frac{\pi}{50}$  rad and  $\phi_s \approx \frac{\pi}{100}$  rad for s- and p-polarization respectively. As a fraction of the full  $2\pi$  phase this gives a maximum deviation from the ideal of 1%, which shows the devices are very robust in terms of their operation with non-normal incident light and have an excellent response at small angles of incidence.

### 2.3. Characterization of Devices and Results

Devices were fabricated using DC and RF sputter deposition, details can be found in Experimental Section. In order to fully characterize the as-fabricated devices a variety of characterization tools were used. First, to verify the devices' deposition consistency the devices were measured using an atomic force microscopy (AFM) device giving information about the quality of the films as-deposited and the thicknesses of layers. This allows us to be confident of the accuracy of the layer thicknesses achieved.

To evaluate the performance of the devices and compare it to simulations, reflection spectra were measured using a microspectrophotometer (JASCO MSV-5300, JASCO Corporation, Tokyo, Japan) between 400 and 700 nm using a Cassegrain  $\times 32$  objective lens with a spot size of 100  $\mu\text{m}$ . Devices were first measured in their as-deposited amorphous state and were re-measured after annealing on a hot plate at  $200^\circ\text{C}$  for 10 min to fully crystallize the GeTe layer.<sup>[39]</sup>

As can be seen in Figure 4a, there is good agreement between the modulation depth of the fabricated devices and the simulated devices across the visible spectrum and, at the specific wavelength of interest (632.8 nm), a modulation depth of 0.38 was

achieved which is in close agreement with the simulation value of 0.39. From this, we find that the devices are performing as expected in terms of amplitude modulation and that the performance at the wavelength of interest is as expected.

Having demonstrated that the optical characteristics of devices crystallized via a hot plate were in good agreement with simulations, the devices were then crystallized through laser scanning. This allows the writing of specific crystalline patterns and images across the spatial extent of the as-deposited amorphous devices. It also mimics the switching that might, ultimately, be carried out in a pixelated device using the aforementioned electrical or embedded heater approaches. In addition it enables the contrast between amorphous and crystalline sections to be viewed directly and, later, will allow us to measure, using single-shot off-axis digital holography, the phase distribution of the light reflected across the sample.

In order to perform laser writing across sections of the devices, a purpose-built optical/electrical test station was used. The instrument uses a 405 nm laser combined with a high numerical aperture objective lens (full details of the test station can be found in Ref. [33]). Crystallization scans of the devices were completed with a laser spot size of approximately  $1 \mu\text{m}^2$ . Figure 4b shows the devices illuminated with white light after a simple pattern featuring a large crystalline square section and two warning-sign-type symbols were written to the device. As can be seen, when illuminated with white light there is very high contrast between the crystalline and amorphous sections.

In order to measure the difference in optical phase between the amorphous and crystalline sections of the device, an off-axis digital holography interferometer was designed and built. Figure 5a shows a simplified diagram of the components and construction of the interferometer and Figure 5b shows a photograph of the optical setup. Off-axis digital holography is a technique that allows the retrieval of both the amplitude and phase of a field pattern with a single image taken using a digital camera.<sup>[40]</sup> The setup has a non-zero angle between the signal beam (that is reflected from the sample) and the reference beam and after digital processing allows for the filtering of the spatial frequencies

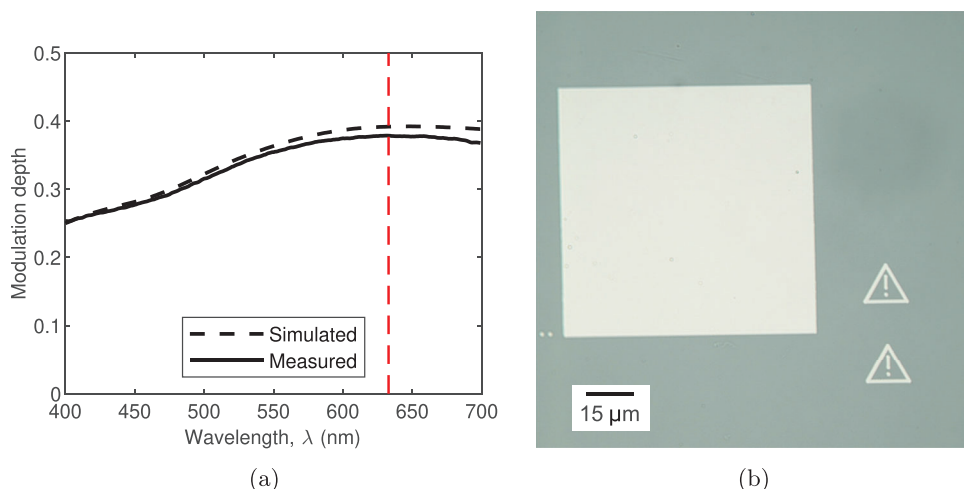


**Figure 4.** a) Simulated and measured modulation depth of the designed and fabricated devices. Good agreement is found between the simulated and measured devices. At the specific wavelength of interest of 632.8 nm (highlighted) a measured modulation depth of 0.38 was achieved from the fabricated devices which is in close agreement with the simulated value of 0.39. b) Devices viewed under a microscope. High contrast can be seen between the amorphous sections of the device (dark) and the crystallized areas of the device (light).

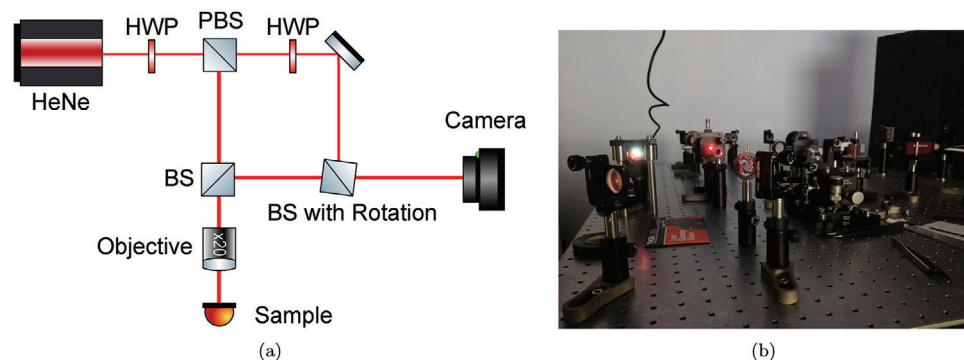


**Figure 5.** a) Experimental setup for measurement of spatial phase difference across the device. This simplified schematic shows sample and reference arms of the off-axis digital holography setup with the rotatable beam splitter to allow for the introduction of a variable angle between the sample and reference beams. Spatial filtering and extraction of phase profile is done digitally. HeNe: Helium Neon Laser. HWP: half-wave plate PSB: polarising beam splitter BS: beam splitter. b) Photograph of off-axis digital holography experimental setup.

present and both the amplitude and phase of the reflected field to be reconstructed. Further details of a standard off-axis digital holography setup can be found in Ref. [40]

**Figure 6** shows reflected spatial intensities and phase measurements of the devices, as obtained using the off-axis digital holography setup. Figure 6a shows the intensity measured, and in which the amorphous and crystalline areas can be clearly seen, and Figure 6b shows a reconstruction of the reflectance (using reflection data from the microspectrophotometer) across a cross section of the sample with both amorphous and crystalline sections. These reflectance plots are compared to Figure 6c–f which show the measured spatial phase distributions across the sample. Figure 6c shows the spatial phase distribution across the same area that is measured in Figure 6a with a  $2\pi$  phase scale; Figure 6e shows the same, but uses a finer phase scale so that small phase differences are visible. Figure 6d shows an averaged cross-section across the device over a  $2\pi$  phase range; Figure 6f shows the same, but again the with the phase magnified.

As can be seen from the measurements, the phase difference of light reflected from the amorphous and crystalline areas is minimal, less than  $\approx\pi/50$  averaged across the measured area, and agrees well with simulation results. In the results shown in Figure 6 it is noted that there are artefacts, arising no doubt from unavoidable dust particles in the optical setup; however, the underlying structures are present and readily measured.

### 3. Conclusion

In summary, we have successfully designed, fabricated, and characterized a phase-change material based amplitude-only constant-phase modulator operating at 632.8 nm. When the PCM is switched between its amorphous and crystalline states, an intensity modulation of 0.38 is achieved with a minimal (averaged) phase modulation of less than  $\approx\pi/50$  across the measured areas.

A laser scanning system was used to write arbitrary patterns and images on to the devices. An off-axis digital holography interferometer was designed and built in order to measure, in a

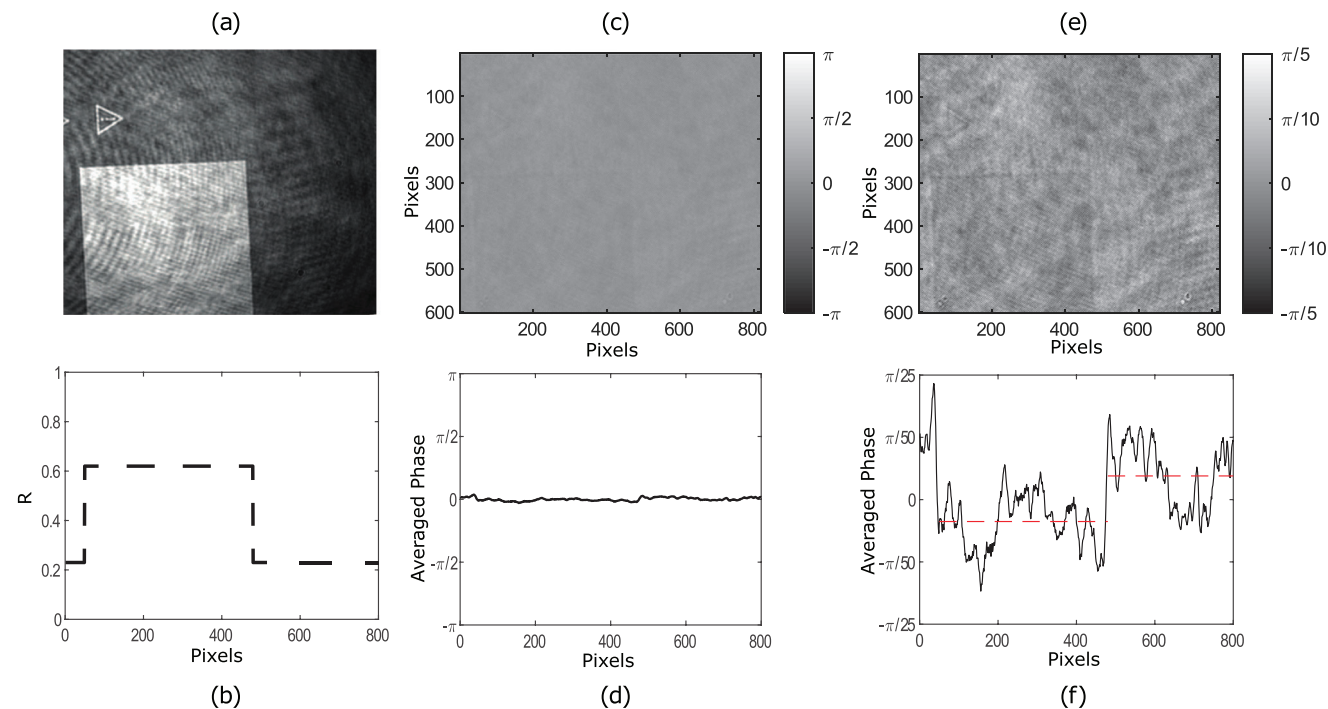


**Figure 6.** Spatial intensity and phase difference across a device with amorphous and laser-written crystalline sections (scale: 100 pixels to 23  $\mu\text{m}$ ). a) Measured intensity. b) Reconstructed intensity distribution using reflection intensities measured in the microspectrophotometer for amorphous ( $R = 0.23$ ) and crystalline ( $R = 0.62$ ) sections. c) Spatial phase distribution across sample (for a  $-\pi$  to  $\pi$  phase scale). d) Averaged phase distribution across crystalline/amorphous boundary (for a  $-\pi$  to  $\pi$  phase scale). e) Spatial phase distribution across sample (for a  $-\pi/5$  to  $\pi/5$  phase scale). f) Averaged phase distribution across crystalline/amorphous boundary (for a  $-\pi/25$  to  $\pi/25$  phase scale).

single shot, the spatial phase distribution across the device and thus fully characterize its operation. The device, in principal, could operate as a fast, solid-state, non-volatile and energy efficient amplitude-only spatial light modulator. The device is designed with ease of fabrication in mind, being a simple thin-film structure with an embedded phase-change material layer. Amplitude-only wavefront modulation can be used to improve coupling efficiency into photonic devices, or to increase the number of degrees of freedom one can control in wavefront shaping, compared with phase-only modulation alone. Our devices have been designed with (ultimately) in-situ switching of PCM layer in mind, thus allowing for the future realization of electrically-controlled pixelated devices.

## 4. Experimental Section

**Fabrication of Thin Film Devices:** Thin film samples were fabricated on Si substrates with an 89 nm  $\text{SiO}_2$  layer. These were cleaned using sonication in acetone and isopropyl alcohol. Layers were deposited using magnetron sputtering using a Moorfield nanoPVD-S10A. Sputtering took place in a chamber with a base pressure of  $7.8 \times 10^{-7}$  mbar with an Ar flow of 1 sccm for a sputtering pressure of  $5.1 \times 10^{-3}$  mbar. First, 100 nm of Ti was sputtered using a DC gun ( $V = 345$  V,  $I = 0.422$  A) at a rate of  $10.24$  nm  $\text{min}^{-1}$ . Next 29 nm of GeTe was sputtered, again with a DC gun ( $V = 422$  V,  $I = 0.016$  A) at a rate of  $5.0$  nm  $\text{min}^{-1}$  and finally the ITO capping layer was sputtered with RF (Forward Power = 45.0 W, Plasma Power = 44.4 W) at a rate of  $2.7$  nm  $\text{min}^{-1}$ . All rates were calibrated by measuring deposited thicknesses on test samples using a Bruker Innova AFM.

## Acknowledgements

J.S. acknowledges funding from the EPSRC CDT in Metamaterials (EP/L015331/1). J.S., J.B., and C.D.W. acknowledge funding from the EPSRC A-META project (EP/W003341/1). C.R.G. acknowledges funding from the Marie Skłodowska-Curie Individual Fellowship 101068089 (METASCALE). The authors would like to thank Dr. Philip Thomas and Prof. Bill Barnes for ellipsometric characterizations.

## Conflict of Interest

The authors declare no conflict of interest.

## Data Availability Statement

The data that support the findings of this study are available from the corresponding author upon reasonable request.

## Keywords

amplitude-only, phase-change materials, reconfigurable, spatial light modulator, thin-film

Received: March 30, 2023

Revised: May 25, 2023

Published online:

- [1] S. Gigan, O. Katz, H. B. De Aguiar, E. R. Andresen, A. Aubry, J. Bertolotti, E. Bossy, D. Bouchet, J. Brake, S. Brasselet, Y. Bromberg, H. Cao, T. Chaigne, Z. Cheng, W. Choi, T. Čižmár, M. Cui, V. R. Curtis, H. Defienne, M. Hofer, R. Horisaki, R. Horstmeyer, N. Ji, A. K. LaViolette, J. Mertz, C. Moser, A. P. Mosk, N. C. Pégard, R. Piestun, S. Popoff, et al., *J. Phys.: Photonics* **2022**, *4*, 042501.
- [2] J. Bertolotti, O. Katz, *Nat. Phys.* **2022**, *18*, 1008.
- [3] C. Rosales-Guzmán, A. Forbes, in *How to Shape Light with Spatial Light Modulators*, SPIE Press, Bellingham, WA, USA **2017**.
- [4] N. Collings, T. Davey, J. Christmas, D. Chu, B. Crossland, *J. Disp. Technol.* **2011**, *7*, 112.
- [5] I. A. Alimi, P. P. Monteiro, A. L. Teixeira, I. A. Alimi, P. P. Monteiro, A. L. Teixeira, in *Telecommunication Systems - Principles and Applications of Wireless-Optical Technologies*, IntechOpen, London **2019**.
- [6] Z. Zhang, Z. You, D. Chu, *Light: Sci. Appl.* **2014**, *3*, e213.
- [7] D. Dudley, W. M. Duncan, J. Slaughter, in *MOEMS Display and Imaging Systems*, Vol. 4985, SPIE, Bellingham, WA, USA, ISSN 0277786X **2003**, p. 14.
- [8] S. Turtaev, I. T. Leite, K. J. Mitchell, M. J. Padgett, D. B. Phillips, T. Čižmár, *Opt. Express* **2017**, *25*, 29874.
- [9] A. P. Mosk, A. Lagendijk, G. Lerosey, M. Fink, *Nat. Photonics* **2012**, *6*, 283.
- [10] H. Cao, A. P. Mosk, S. Rotter, *Nat. Phys.* **2022**, *18*, 994.
- [11] H. Yang, D. P. Chu, *J. Phys.: Photonics* **2020**, *2*, 032001.
- [12] A. B. Ayoub, D. Psaltis, *Sci. Rep.* **2021**, *11*, 1.
- [13] I. M. Vellekoop, A. P. Mosk, *Opt. Lett.* **2007**, *32*, 2309.
- [14] C. R. de Galarreta, S. G. Carrillo, Y. Y. Au, E. Gemo, L. Trimby, J. Shields, E. Humphreys, J. Faneca, L. Cai, A. Baldycheva, J. Bertolotti, C. D. Wright, *J. Opt.* **2020**, *22*, 20.
- [15] S. V. Makarov, A. S. Zalogina, M. Tajik, D. A. Zuev, M. V. Rybin, A. A. Kuchmizhak, S. Juodkazis, Y. Kivshar, *Laser Photonics Rev.* **2017**, *11*, 5.
- [16] J. Siegel, A. Schropp, J. Solis, C. N. Afonso, M. Wuttig, *Appl. Phys. Lett.* **2004**, *84*, 2250.
- [17] I. S. Kim, S. L. Cho, D. H. Im, E. H. Cho, D. H. Kim, G. H. Oh, D. H. Ahn, S. O. Park, S. W. Nam, J. T. Moon, C. H. Chung, in *Digest of Technical Papers - Symp. on VLSI Technol.*, IEEE, Honolulu, HI, USA, ISBN 9781424476374, ISSN 07431562, **2010**, pp. 203–204.
- [18] Y. Chen, S. Mu, G. Wang, X. Shen, J. Wang, S. Dai, T. Xu, Q. Nie, R. Wang, *Appl. Phys. Express* **2017**, *10*, 105601.
- [19] S. Raoux, G. W. Burr, M. J. Breitwisch, C. T. Rettner, Y. C. Chen, R. M. Shelby, M. Salinga, D. Krebs, S. H. Chen, H. L. Lung, C. H. Lam, *IBM J. Res. Dev.* **2008**, *52*, 465.
- [20] M. Wuttig, N. Yamada, *Nat. Mater.* **2007**, *6*, 824.
- [21] S. Raoux, H. Y. Cheng, M. A. Caldwell, H. S. Wong, *Appl. Phys. Lett.* **2009**, *95*, 071910.
- [22] C. R. de Galarreta, I. Sinev, A. M. Alexeev, P. Trofimov, K. Ladutenko, S. Garcia-Cuevas Carrillo, E. Gemo, A. Baldycheva, J. Bertolotti, C. David Wright, *Optica* **2020**, *7*, 476.
- [23] J. Shields, C. R. de Galarreta, J. Bertolotti, C. David Wright, *Nanomaterials* **2021**, *11*, 525.
- [24] C. Rios, M. Stegmaier, P. Hosseini, D. Wang, T. Scherer, C. D. Wright, H. Bhaskaran, W. H. Pernice, *Nat. Photonics* **2015**, *9*, 725.
- [25] C. R. de Galarreta, A. Alexeev, J. Bertolotti, C. D. Wright, in *Proc. IEEE Int. Symp. on Circuits and Syst.*, Institute of Electrical and Electronics Engineers, Florence, Italy, ISBN 9781538648810, ISSN 02714310, **2018**, pp. 1–5.
- [26] S. G. C. Carrillo, L. Trimby, Y. Y. Au, V. K. Nagareddy, G. Rodriguez-Hernandez, P. Hosseini, C. Rios, H. Bhaskaran, C. D. Wright, *Adv. Opt. Mater.* **2019**, *7*, 1801782.
- [27] M. Wuttig, H. Bhaskaran, T. Taubner, *Nat. Photonics* **2017**, *11*, 465.
- [28] P. Hosseini, C. D. Wright, H. Bhaskaran, *Nature* **2014**, *511*, 206.
- [29] K. Shportko, S. Kremers, M. Woda, D. Lencer, J. Robertson, M. Wuttig, *Nat. Mater.* **2008**, *7*, 653.
- [30] M. Krbal, A. V. Kolobov, P. Fons, K. Nitta, T. Uruga, J. Tominaga, *Pure Appl. Chem.* **2019**, *91*, 1769.
- [31] E. Gourvest, B. Pelissier, C. Vallée, A. Roule, S. Lhostis, S. Maitrejean, *J. Electrochem. Soc.* **2012**, *159*, H373.
- [32] A. N. Kolb, N. Bernier, E. Robin, A. Benayad, J. L. Rouvière, C. Sabbione, F. Hippert, P. Noe, *ACS Appl. Electron. Mater.* **2019**, *1*, 701.
- [33] Y.-Y. Au, H. Bhaskaran, C. D. Wright, *Sci. Rep.* **2017**, *7*, 9688.
- [34] Y. Zhang, C. Fowler, J. Liang, B. Azhar, M. Y. Shalaginov, S. Deckoff-Jones, S. An, J. B. Chou, C. M. Roberts, V. Liberman, M. Kang, C. Rios, K. A. Richardson, C. Rivero-Baleine, T. Gu, H. Zhang, J. Hu, *Nat. Nanotechnol.* **2021**, *16*, 661.
- [35] E. Gemo, S. V. Kesava, C. Ruiz De Galarreta, L. Trimby, S. Garcia-Cuevas Carrillo, M. Riede, A. Baldycheva, A. Alexeev, C. D. Wright, *Opt. Mater. Express* **2020**, *10*, 1675.
- [36] P. B. Johnson, R. W. Christy, *Phys. Rev. B* **1974**, *9*, 5056.
- [37] M. Kang, I. Kim, M. Chu, S. W. Kim, J.-W. Ryu, *J. Korean Phys. Soc.* **2011**, *59*, 3280.
- [38] D. H. Kim, F. Merget, M. Laurenzis, P. H. Bolivar, H. Kurz, *J. Appl. Phys.* **2005**, *97*, 083538.
- [39] J. Pries, Y. Yu, P. Kerres, M. Häser, S. Steinberg, F. Gladisch, S. Wei, P. Lucas, M. Wuttig, *Phys. Status Solidi RRL* **2021**, *15*, 2000478.
- [40] E. Cuche, P. Marquet, C. Depeursinge, *Appl. Opt.* **2000**, *39*, 4070.